Miner Deposita (2009) 44:41–59
DOI 10.1007/s00126-007-0153-3

ARTICLE

Geochronology of unconformity-related uranium deposits in the Athabasca Basin, Saskatchewan, Canada and their integration in the evolution of the basin

Paul Alexandre · Kurt Kyser · Dave Thomas · Paul Polito · Jim Marlat

Received: 30 January 2006 / Accepted: 10 June 2007 / Published online: 31 July 2007

Abstract The importance of geochronology in the study of mineral deposits in general, and of unconformity-type uranium deposits in particular, resides in the possibility to situate the critical ore-related processes in the context of the evolution of the physical and chemical conditions in the studied area. The present paper gives the results of laser step heating $^{40}Ar/^{39}Ar$ dating of metamorphic host-rock minerals, pre-ore and syn-ore alteration clay minerals, and laser ablation inductively coupled plasma mass spectrometer (LA-ICP-MS) U/Pb dating of uraninite from a number of basement- and sediment-hosted unconformity-related deposits in the Athabasca Basin, Canada. Post-peak metamorphic cooling during the Trans-Hudson Orogen of rocks from the basement occurred at ca 1,750 Ma and gives a maximum age for the formation of the overlying Athabasca Basin. Pre-ore alteration occurred simultaneously in both basement- and sandstone-hosted mineralizations at ca 1,675 Ma, as indicated by the $^{40}Ar/^{39}Ar$ dating of pre-ore alteration illite and chlorite. The uranium mineralization age is ca 1,590 Ma, given by LA-ICP-MS U/Pb dating of uraninite and $^{40}Ar/^{39}Ar$ dating of syn-ore illite, and is the same throughout the basin and in both basement- and sandstone-hosted deposits. The mineralization event, older than previously proposed, as well as several fluid circulation events that subsequently affected all minerals studied probably correspond to far-field, continent-wide tectonic events such as the metamorphic events in Wyoming and the Mazatzal Orogeny (ca 1.6 to 1.5 Ga), the Berthoud Orogeny (ca 1.4 Ga), the emplacement of the McKenzie mafic dyke swarms (ca 1.27 Ga), the Grenville Orogeny (ca 1.15 to 1 Ga), and the assemblage and break-up of Rodinia (ca 1 to 0.85 Ga). The results of the present work underline the importance of basin evolution between ca 1.75 Ga (basin formation) and ca 1.59 Ga (ore deposition) for understanding the conditions necessary for the formation of unconformity-type uranium deposits.

Keywords Unconformity-type uranium deposits · Geochronology · Basin evolution · Athabasca Basin · Canada

Editorial handling: M. Cuney

Electronic supplementary material The online version of this article (doi:10.1007/s00126-007-0153-3) contains supplementary material, which is available to authorized users.

P. Alexandre (✉) · K. Kyser · P. Polito
Department of Geological Sciences and Geological Engineering,
Queen's University,
Kingston, ON, Canada K7L 3N6
e-mail: alexandre@geol.queensu.ca

K. Kyser
e-mail: kyser@geol.queensu.ca

P. Polito
e-mail: PaulPolito@angloamerican.com.au

D. Thomas · J. Marlat
Cameco Corporation,
2121, 11th Street West,
Saskatoon, SK, Canada S7M 1J3

D. Thomas
e-mail: dave_thomas@cameco.com

J. Marlat
e-mail: jim_marlat@cameco.com

Introduction

Unconformity-type uranium deposits provide much of the world stock of uranium (Robertson et al. 1978; Sibbald and Quirt 1987). Most of these ore-bodies are sediment-hosted, situated in the sandstones immediately above the sediment-basement unconformity, whereas others are basement-

hosted, situated in the basement rocks below the unconformity. The age of unconformity-type uranium deposits in the Athabasca Basin, Canada has been addressed early on, as it is central to the understanding their formation. Indeed, understanding the ore formation processes necessitates knowing the time of deposit formation so that the exact physical and chemical characteristics prevailing then can be put into context.

The relative timing of ore formation events for unconformity-type uranium deposits has been addressed via paragenetic studies (e.g., Hoeve and Sibbald 1978; Fayek and Kyser 1997), whereas the absolute timing has been studied using various isotopic systems. The proposed absolute ages for the uranium deposits in the Athabasca Basin vary widely from ca 900 to ca 1,400 Ma and obtained mostly by U/Pb dating of uraninite and pitchblende (e.g., Carl et al. 1992; Philippe et al. 1993; Baagsgard et al. 1984) and $^{40}Ar/^{39}Ar$ and K–Ar dating of illite associated with uranium mineralization (e.g., Bray et al. 1988). On the basis of these ages, Cumming and Kristic (1992) proposed that the formation of the uranium deposits occurred between 1,330 and 1,380 Ma. However, more recent U/Pb dating of uraninite using the enhanced spatial resolution of the ion-probe method yield upper intercept ages of 1,519±22 Ma for the sandstone-hosted deposit at McArthur River (Fayek et al. 2002) and 1,467±47 Ma for the sandstone-hosted deposit at Cigar Lake (Fayek et al. 2002), comparable to the recent conventional U/Pb age of 1,521±8 Ma obtained for the sandstone-hosted deposit at McArthur River (McGill et al. 1993).

Dating of uraninite is challenging, as it is chemically very active in most conditions and recrystallizes readily in low temperature conditions (Finch and Murakami 1999; Fayek and Kyser 2000; Alexandre and Kyser 2005), releasing part or all of the radiogenic Pb it has accumulated. The associated clay minerals are also difficult to date, as they have poor argon retention because of small grain size and low crystallinity (McDougall and Harrison 1999). These complications suggest that some previously published absolute ages of unconformity-type uranium deposits may have been biased as a result of radiogenic Pb and Ar loss, which produces lower ages and, thus, explains the large variation in the ages previously published.

In this study, results from U/Pb dating of uraninite and $^{40}Ar/^{39}Ar$ dating of clay minerals from three basement-hosted unconformity-type uranium deposits and from several sediment-hosted unconformity-type uranium mineralizations from the Athabasca Basin in Canada are presented. The basement-hosted deposits include those at Rabbit Lake, Dawn Lake, and the basement-hosted ore-body of McArthur River deposit. Results are also presented for the sandstone-hosted part of the McArthur River deposit, Virgin River Southwest, and Hook Lake sandstone-hosted prospects, and the deep drill-hole VR01, which is not mineralized and is regarded as corresponding to typical background alteration in the Athabasca Group. The methods used are U/Pb dating of uranium-rich minerals by laser ablation high-resolution inductively coupled plasma mass spectrometer (LA-HR-ICP-MS) and laser-probe step heating argon–argon dating of phyllosilicate minerals ($^{40}Ar/^{39}Ar$). The results obtained not only reveal the age of the primary uranium mineralization but also times the deposits, and prospects were perturbed by fluid events during the evolution of the Athabasca Basin.

Geological context

The basement-hosted deposits studied at McArthur River, Dawn Lake, and Rabbit Lake are situated on the eastern margin of the Athabasca Basin (Fig. 1) and are hosted by Archean and Aphebian basement rocks. The sandstone-hosted prospects at Virgin River, Southwest, Hook Lake, and the background drill-hole VR01 are situated in the south central and western part of the Athabasca Basin and are hosted by the sediments of the Athabasca Group (Fig. 1).

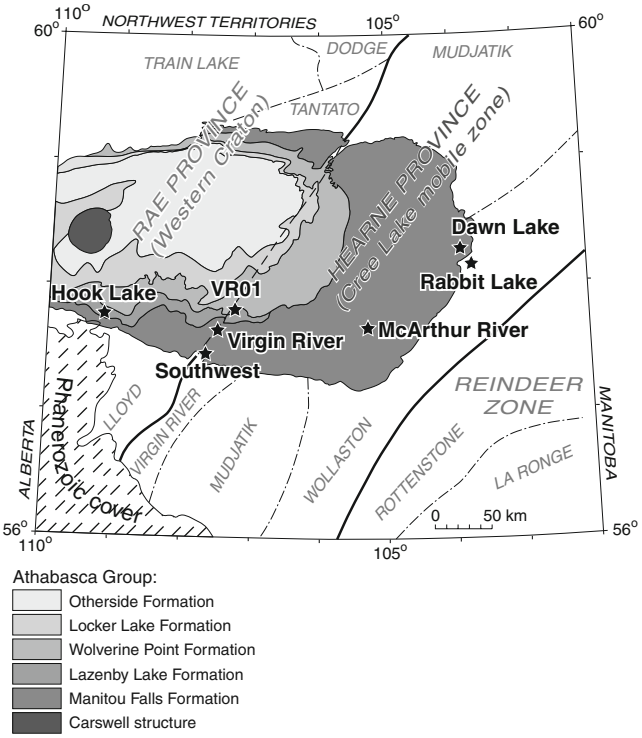

Fig. 1 Simplified geological map of northern Saskatchewan, Canada. The major lithotectonic units of its basement (provinces and their domains) are indicated in *italics*. The formations of the Athabasca Group are indicated in *gray levels*. The positions of the basement- and sediment-hosted uranium mineralizations studied are shown. Modified from Hoeve and Sibbald (1978), Sibbald and Quirt (1987), and Ramaekers (1990)

Basement

The basement comprises Archean and Paleoproterozoic rocks that were previously metamorphosed during the Trans-Hudson Orogen (Lewry and Sibbald 1980). These are part of the Wollaston and the Virgin River Domains of the larger Cree Lake mobile zone which is situated between the Western Craton and the Reindeer Zone (Fig. 1). The Wollaston Domain is a northeast-trending fold and thrust belt that is fault-bounded to the east by the Peter Lake and the Rottenstone domains and to the west by the Mudjatik Domain (Money 1968; Fig. 1). The Wollaston Domain comprises older Archean granitoid gneisses and an Early Paleoproterozoic sequence (Wollaston Group) that has been intensely deformed during the Trans-Hudson Orogen (Money 1968). Four main groups of rocks are distinguished in the basement complex (Lewry and Sibbald 1977): (1) Archean granitic, granodioritic, and tonalitic orthogneisses and subordinate metamorphic rocks, (2) high-grade Paleoproterozoic Wollaston Group metasedimentary rocks, (3) deformed calc-alkaline granitoids and minor gabbros, and (4) peraluminous granitoids of different petrochemical types.

The Wollaston Group was deposited unconformably on Archean crust before any proximal Paleoproterozoic orogenic events (Money 1968). It is predominantly of sedimentary origin and is composed predominantly of graphitic and non-graphitic pelitic, psammopelitic, and psammitic gneisses, subordinate metaquartzite, calc-silicates, and amphibolites, as well as rare BIF (Lewry and Sibbald 1980). Rocks of the Wollaston Group were complexly deformed and metamorphosed by the Trans-Hudson Orogen, which reached peak metamorphism at ca 1,800–1,820 Ma (Lewry and Sibbald 1980; Kyser et al. 2000). Subsequent rapid uplift began at ca 1,750 Ma as recorded by K–Ar and $^{40}Ar/^{39}Ar$ cooling ages (Burwash et al. 1962; Kyser et al. 2000).

Athabasca Group sediments

The Athabasca Basin formed at ca 1,730 Ma as a series of NE–SW oriented sub-basins (Armstrong and Ramaekers 1985; Kyser et al. 2000). Basin fill consists of thick clastic sequences of Paleoproterozoic age resulting from the rapid exhumation of the Trans-Hudson Orogenic Belt (Ramaekers 1990). The basin is subdivided into three sub-basins, with most of the uranium deposits located in the easternmost Cree sub-basin. The Athabasca Basin consists of sequences of Helikian polycyclic, mature fluvial to marine quartz sandstone, collectively referred to as the Athabasca Group. These were deposited in a near-shore shallow shelf environment (Ramaekers and Dunn 1977; Ramaekers 1990). The basal sequence of the Athabasca Group (Manitou Falls and Fair Point formations) consists of coarse to fine-grained hematite-rich conglomerates and silty sandstones that filled the sub-basins and combine to form the full extent of the Athabasca Basin. In the Manitou Falls Formation, hematization occurs along thin stratigraphic horizons, indicating oxidation of heavy mineral layers. The basal sandstones are overlain by an arkosic succession of less permeable marine sandstones, fluor-apatite siltstones, and phosphatic mudstones (the Lazenby Lake, Wolverine Point, Locker Lake, Otherside and Tuma Lake formations, respectively), which are, in turn, overlain by a series of shales (Douglas Formation) and stromatolic dolomites (Carswell Formation). The Athabasca Basin is presently 1 to 2 km thick; however, temperature estimates from fluid inclusions indicate that the sedimentary sequence may have reached a thickness of 5 to 6 km during the mid Proterozoic (Pagel et al. 1980).

The Athabasca Group sedimentary rocks and the basement complex are cut by a series of northwestly trending mafic dykes known as the McKenzie dyke swarms (Cumming and Kristic 1992). The dyke trend corresponds to tensional directions associated with left-lateral movement along the ancient Hudsonian faults (Hoeve and Sibbald 1978; Sibbald and Quirt 1987). These intrusives range in size from 1 m to several hundred meters wide and have an U–Pb age of 1,267±2 Ma (LeCheminant and Heaman 1989).

Deposits and prospects studied

Basement-hosted deposits

The McArthur River deposit is made of three sediment-hosted and one basement-hosted ore bodies. It is the world's largest high-grade uranium deposit. The basement-hosted P2 ore body, which is the object of the present study, contains half of the uranium in the deposit (McGill et al. 1993). The sub-Athabasca basement host rocks consist of two distinct metasedimentary sequences: (1) a hanging wall pelitic sequence of cordierite- and graphite-bearing pelitic and psammitopelitic gneiss with a minor meta-arkose and calc-silicate gneisses and (2) a sequence consisting of meta-quartzite and silicified meta-arkose and rare pelitic gneisses (McGill et al. 1993). This deposit (Fig. 2) is characterized by an abrupt transition from nearly unaltered basement host rock to intense chloritic alteration and then to the mono-mineralic high-grade uranium mineralization (McGill et al. 1993). Two uranium-rich whole rock samples have been dated by the U/Pb method and give discordia ages of 1,348±16 and 1,521±8 Ma, the older being interpreted as the age of the primary uranium mineralization and the younger as the age of a remobilization event (McGill et al. 1993).

The Dawn Lake deposit consists of four zones, 11, 11A, 11B, and 14, with the two most important being 11A and

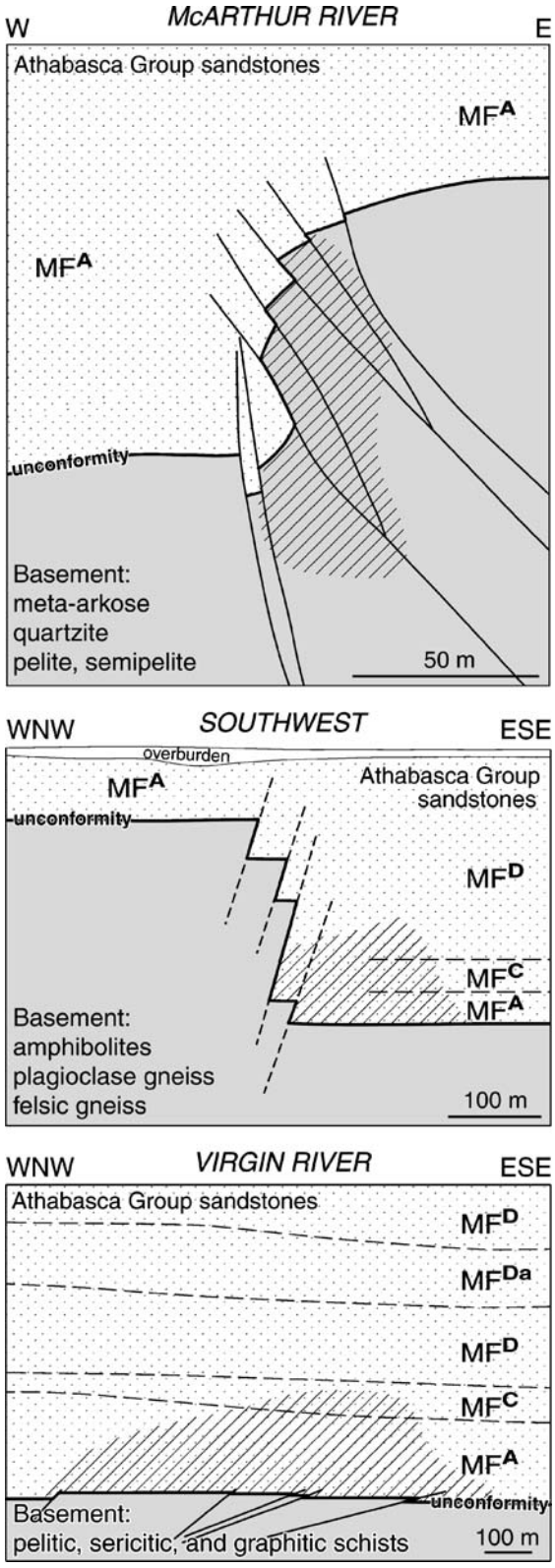

Fig. 2 Simplified schematic cross-sections of three of the studied zones showing the major lithologies present. The *dashed areas* indicate the most intense alteration and the associated uranium mineralization. After McGill et al. (1993) and Alexandre et al. (2005), modified

11B, which are the object of this study. There are four separate NE–SW elongated, cigar-shaped ore bodies in zone 11A, and three in 11B, each being between 100 and 190 m long and 20 to 45 m wide. The Dawn Lake deposit is hosted by metapelites, calc-silicates, crenulites, biotite gneisses, and pegmatites of the Wollaston Group (Chan et al., unpublished Cameco Corp. report). Alteration of the basement rocks around the deposit consists mainly of chloritization and illitization (Quirt 1997). The orientation of the main controlling structure is a steeply west dipping strike-slip fault system with predominantly horizontal displacement (Chan et al., unpublished Cameco Corp. report). This structure makes the Dawn Lake deposit atypical of basement-hosted unconformity-type deposits in the eastern Athabasca basin, which are controlled by major NNE/SSE oriented thrust-fault systems.

The Rabbit Lake deposit is hosted by Aphebian Wollaston Group supracrustals comprising interlayered meta-arkoses and calc-silicates in the hanging wall (upper gneisses), massive meta-arkose in the core of the ore zone, and partly graphitic plagioclasite, calc-silicates and dolomitic marbles in the footwall (Wallis 1971; Knipping 1974; Chandler 1978). Evidence of faulting is widespread, and two major structures are recognized. The younger, the Rabbit Lake thrust fault, underlies the deposit, dips 30° SSE, and downthrows the Athabasca Group sediments to the northeast at least 75 m against the crystalline basement. An older northeasterly trending and steeply dipping fault bounds the ore zone to the southeast (Sibbald 1978). A high-grade core is surrounded by a lower grade envelope of mineralization (Hoeve and Sibbald 1978). Mineralization comprises several different generations of uraninite and coffinite, accompanied by several other minerals including euhedral quartz, dolomite, calcite, hematite, chlorite, and sulfides.

Despite some differences, alteration assemblages of these three basement-hosted deposits are overwhelmingly similar, enabling one paragenetic sequence to adequately describe all of the deposits studied (Alexandre et al. 2004). The earliest alteration phase involves intense illitization of feldspar (Fig. 3a) and amphibole followed by alteration of biotite and illite to chlorite (Fig. 3b) that is typically blue under polarized light. The relative abundance of illite and chlorite vary in space with illite predominant distal to the ore zone and chlorite predominant proximal to the orebody. Uranium mineralization is manifest as uraninite (U^1; Fig. 3c and 4a), which is the only uranium mineral to form at this stage. It is massive at the McArthur River deposit (Fig. 3c) and precipitates in voids and open fractures created by pre-ore alteration at the Dawn Lake and the Rabbit Lake deposits where it forms a more disseminated mineralization. Uraninite crystals are often euhedral to sub-euhedral or colloform (Fig. 3c), particularly at the McArthur River deposit, or have irregular shape as at the Dawn Lake and the

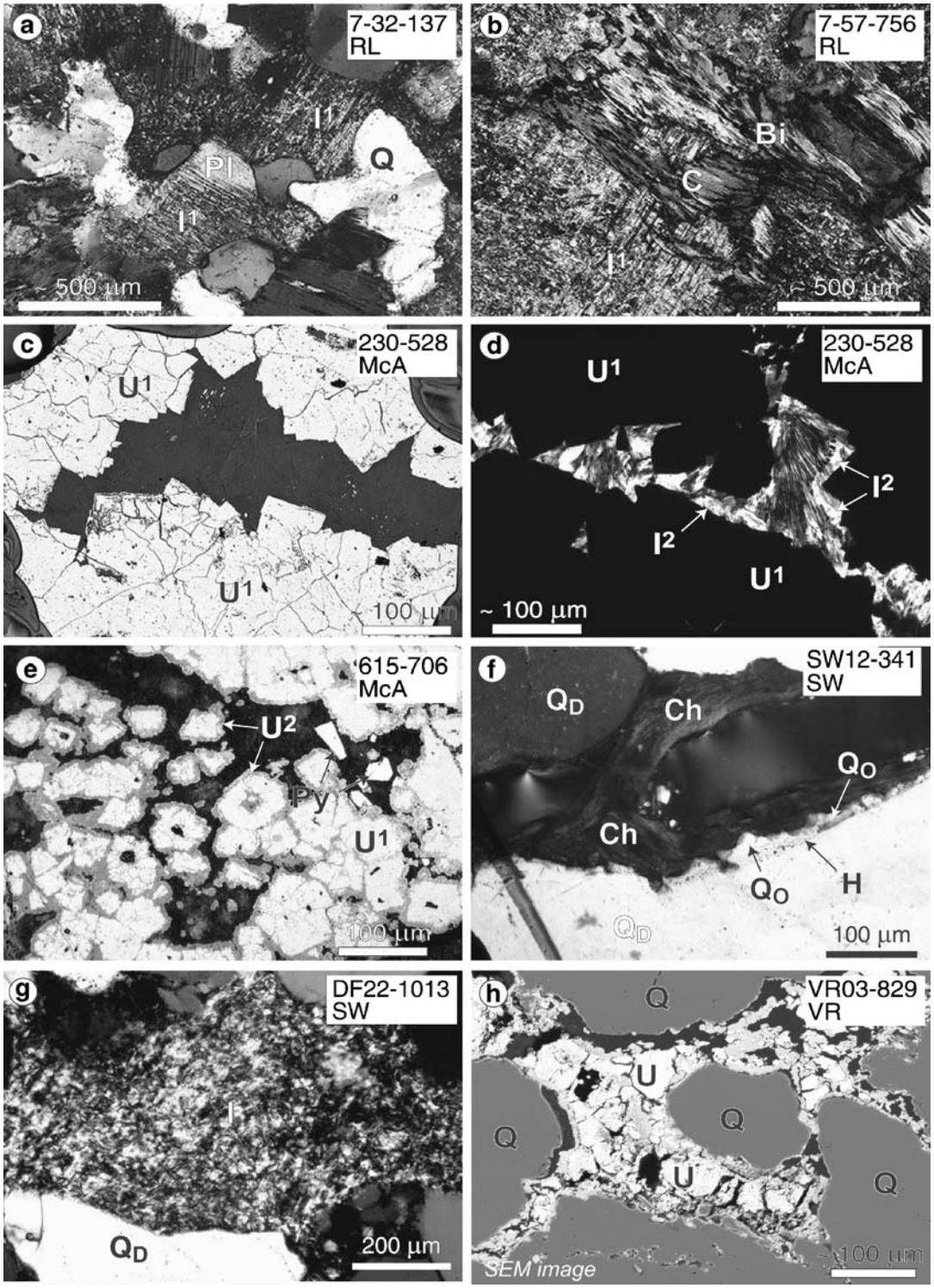

Fig. 3 Photomicrographs of typical mineral assemblages from the uranium deposits studied. **a** to **e** Basement-hosted deposits; **f** to **g** sandstone-hosted deposits and prospects. **a** Pre-ore illitization (I^1) of plagioclase (*Pl*); biotite is not yet altered (transmitted light). **b** Pre-ore chloritization (*C*) of biotite (*Bi*), all other minerals are illitized (I^1) (transmitted light). **c** Euhedral and visually homogeneous uraninite (U^1) in reflected light. **d** Syn-ore coarse-grained illite (I^2) accompanying uraninite (U^1) (transmitted light). **e** Euhedral uraninite (U^1) with altered rims (U^2) and post-ore pyrite (reflected light). **f** Hematite (*H*) and quartz overgrowth (Q_O) over detrital quartz (Q_D), with chlorite (*Ch*) precipitated in the open space, in transmitted light. **g** Strong pervasive illite (*I*) alteration in pore space between quartz grains (*Q*) in transmitted light. **h** Uraninite grains (*U*) situated in pore space between quartz (*Q*) (SEM image). Also shown are the sample number and the deposit (*McA* McArthur River, *RL* Rabbit Lake, *VR* Virgin River, *SW* Southwest)

Rabbit Lake deposits. Coarse-grained, 30 to 50 μm euhedral illite (I^2) is the only phase that accompanies uraninite precipitation (Fig. 3d). Post-ore alteration is manifest as vein chlorite, euhedral quartz, spherulitic dravite, dolomite, and rare kaolinite (Fig. 4a). Uraninite is often partially altered to coffinite (Alexandre and Kyser 2005) and a new uraninite generation (U^2; Fig. 3e) with a concomitant release of radiogenic Pb, which precipitates as microscopic (<5 μm) grains of galena within the uraninite. Pyrite, rutile, and rare chalcopyrite, bornite, pentlandite, cobaltite, and magnetite precipitate late as disseminated euhedral to sub-euhedral grains with sizes up to 100 μm (Fig. 4a).

Sandstone-hosted prospects

The Athabasca Group is represented by the Manitou Falls Formation (MFa, MFb, MFc, and MFd members), Lazenby Lake Formation (LzL), and Wolverine Point Formation (Wpa and WPb members; Ramaekers and Dunn 1977; Ramaekers 1990). In the central south part of the basin where the Virgin River and Southwest prospects and the background drill-hole VR01 (Fig. 1) are situated, only the Manitou Falls Formation is present, overlying the Virgin River Domain basement rocks that consist of graphitic pelitic schists, fine-grained amphibolites, felsic gneiss, plagioclase gneiss, and deformed granitoids (Fig. 2; Chandler 1978). The thickness of the Athabasca Group varies from ca 1,000 m at VR01, 800 to 900 m at Virgin River, and down to ca 200 m at Southwest (Fig. 2). The MFa part of the sequence is represented by interbedded matrix-supported quartz pebble conglomerate and poorly sorted medium-grained sandstone. The MFb member is dominated by medium-grained quartz sandstone along with a substantial component of poorly sorted and clast-supported conglomeratic sandstone and is only rarely present in the area. The MFc member is a relatively clean medium- to coarse-grained sandstone with narrow (<2 cm) granule and pebble beds. The MFd member is also a relatively clean, medium- to coarse-grained sandstone, but contains a significant amount of clay interclasts.

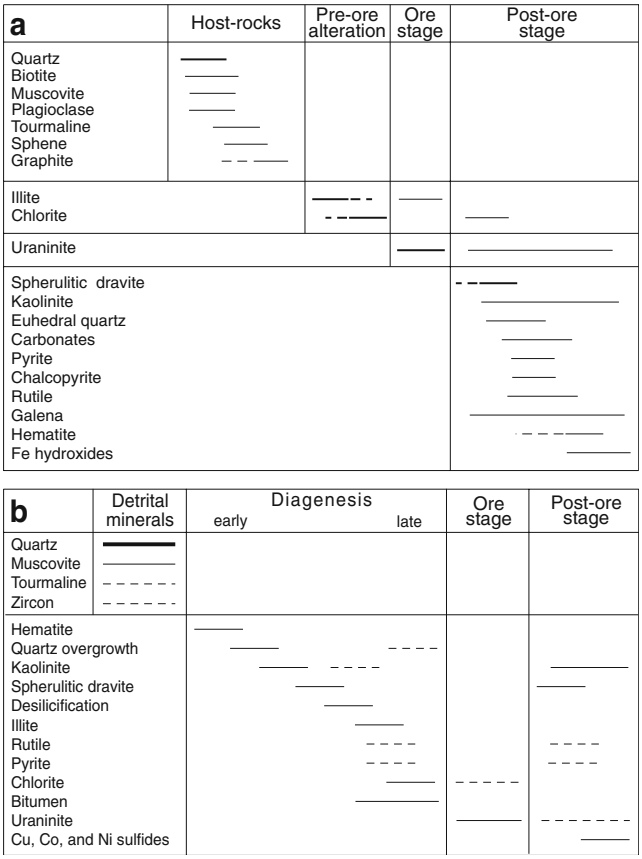

Fig. 4 Simplified paragenesis for the unconformity type uranium mineralizations in the Athabasca Basin. **a** Basement-hosted deposits, **b** sediment-hosted mineralizations. The *thickness* of the lines indicates the relative abundance, while *dashed lines* indicate uncertain position in the paragenesis of the corresponding minerals

The major structural feature here is the major NE–SW oriented Dufferin Lake fault, which is part of the major Virgin River fault zone, and extends to more than 50 km from north to south. Further west, at Hook Lake, the Athabasca Group includes the Lazenby Lake Formation (LzL) and the Wolverine Point Formation (Wpa and WPb members). The Lazenby Lake Formation discomfortably overlies the MFd and is marked by medium- to coarse-grained pebbly sandstones containing pebbles larger or equal to 4 mm. The Wolverine Point Formation sandstones comfortably overlie the LzL and consist of medium- to very coarse-grained quartz arenites. The basement here is part of the Western Granulite Domain of the Archean Rae Province and consists of gneisses with subordinate amounts of anorthosite, quartzite, and pelite. Non-economic uranium mineralization has been found at Virgin River and Southwest as disseminated uraninite grains, whereas Hook Lake and VR01 are barren.

The general paragenesis in the sandstone-hosted prospects is dominated by diagenetic and hydrothermal alteration. Early diagenesis during initial burial is characterized by hematite staining (indicating oxidizing fluids) preceding quartz overgrowths and the precipitation of fine-grained kaolinite and minor spherulitic dravite (Fig. 4b). Desilicification is manifest as quartz dissolution accompanied by minor coarse-grained kaolinite. Near the uranium mineralization, pre-ore alteration is manifest as illite (Fig. 3g) preceding minor pyrite and rutile, indicating reducing conditions, followed by chlorite (Fig. 3f) and minor euhedral quartz formed in open fractures (Fig. 4b). One particularity of the Southwest prospect is the presence of early bitumen (Fig. 4b) probably formed during late diagenesis. It served as reductant for uraninite precipitation resulting in a mixture of very fine-grained uraninite and globular bitumen and uraniferous bitumen (Alexandre and

Kyser 2006). The ore stage is characterized by disseminated uraninite grains not exceeding 0.5 mm across (Fig. 3h), rimmed by chlorite in the case of Southwest. The post-ore stage is characterized by additional kaolinite and a minor amount of spherulitic dravite, pyrite and rutile, and locally abundant copper, nickel, and cobalt sulphides (Fig. 4b). Several stages of uraninite alteration and recrystallization can be distinguished. The two non-mineralized areas, Hook Lake and VR01, are, in general, characterized by the absence of pyrite, much lower amounts of clay alteration in general and chlorite in particular, and the absence of coarse-grained kaolinite.

Dating methodology

U/Pb dating of uranium-rich minerals by U/Pb LA-HR-ICP-MS

The U/Pb dating of uraninite samples is performed on polished thin sections. All samples were examined by reflected light microscopy, and only those showing no visible signs of recrystallization (i.e., those with the highest reflectance) were selected for the LA-HR-ICP-MS analysis. The laser used is the Mercantek® LUV213 laser ablation system with a frequency quintupled Nd-YAG (213 nm) used mostly in spot mode. The laser conditions included laser power output of 30 to 40% (<1 mJ/cm^2), pulses of 50 ms with repetition rate of 2 Hz, and spot size of 25 to 35 μm. The HR-ICP-MS instrument used is a double-focusing Finnigan MAT Element®, with the magnetic sector located in front of the electrostatic analyzer. The gas (argon in all cases) flows were as follows: cooling gas, 14 l/min; auxiliary gas, 0.8 l/min; sample carrier gas, 1.2 l/min. The forward power is 1,250 W and the reflected power less than 7 W. Medium mass resolution of 4,500 (defined as the ratio of mass over peak width at 5% of the signal height) was used (Kyser et al. 2003). The acquisition mode is peak-jumping, and the analyzer is a secondary electron multiplier (SEM). The isotopes measured are ^{201}Hg, ^{202}Hg (used for correction for interferences of ^{204}Hg on ^{204}Pb), ^{204}Pb (used for common Pb correction), ^{206}Pb, ^{207}Pb, ^{208}Pb, ^{235}U, and ^{238}U. One analysis consisted of ten cycles of measures of these isotopes, with measuring times of 1.1 ms (for ^{201}Hg, ^{202}Hg, ^{206}Pb, and ^{238}U), 20 msec (for ^{204}Pb), 4 ms (for ^{207}Pb and ^{208}Pb), and 6 ms (for ^{235}U). The signals obtained vary from hundreds of counts per second (cps) for the Hg isotopes to millions of cps for the uranium isotopes. The instrumental mass bias, as checked against the international zircon standard 91500, is negligible. The matrix effect was too low to be detected at the present level of analytical precision. The ages were checked against an in-house 1,480 Ma davidite standard. Further analytical details, as well as a description of dating uraninite and comments about its particular challenges, are given in Chipley et al. (2007).

Laser-probe step heating argon dating of phyllosilicate minerals (^{40}Ar/^{39}Ar)

^{40}Ar/^{39}Ar analyses were performed on handpicked individual grains of coarse-grained sericite and millimeter-sized aggregates of illite or muscovite and on micrometer-sized illite and chlorite fractions separated by ultrasound disintegration of whole sample and centrifugation. All separates were analyzed by X-ray diffraction (XRD) to verify purity.

Mineral separates and flux monitors (hornblende standard Hb3Gr with age of 1,071 Ma; Roddick 1983) were wrapped in Al foil, and the resulting packets were stacked vertically into the Al container and then irradiated with fast neutrons in the McMaster University Nuclear Reactor for 120 h. Flux monitors were located at ca 1-cm intervals along the irradiation container, and J values for individual samples were determined by second-order polynomial interpolation between the monitors. For total fusion of monitors and step heating of samples, an 8-W Lexel 3500 continuous argon-ion laser was used (Lee et al. 1990). For step heating, the laser beam was defocused to cover the entire sample. Heating periods were ca 3 min at increasing power settings (0.2 to 7 W). The released gas, after purification using an SAES C50 getter for 5 min, was admitted to an online MAP 216 mass spectrometer, with a Båur Signer source and an electron multiplier. Blanks, measured before every sample, were subtracted from the subsequent sample gas-fractions. The extraction blanks were typically $<10\times10^{-13}$, $<0.5\times10^{-13}$, $<0.5\times10^{-13}$, and $<0.5\times10^{-13}$ cm^{-3} STP for masses 40, 39, 37, and 36, respectively. Measured argon isotope signals were extrapolated to zero time. Contaminant atmospheric argon was subtracted using measured ^{40}Ar/^{36}Ar atmospheric ratios, and the argon isotopes were corrected for neutron-induced ^{40}Ar from potassium, ^{39}Ar and ^{36}Ar from calcium (Onstott and Peacock 1987), and ^{36}Ar from chlorine (Roddick 1983). Ages and error margins were calculated using the methods of Dalrymple et al. (1981) and constants recommended by Steiger and Jåger (1977).

For several samples, plateau ages were calculated using not less of 70% of the gases released and three consecutive steps that overlap in their 1 σ error margin. In some cases, pseudo-plateau ages were calculated, defined either on a shorter portion of the gas or on only two steps. When these conditions were not met, an average age based on a relatively flat portion of the spectrum was proposed.

The age information obtained using ^{40}Ar/^{39}Ar dating of clay minerals is often difficult to interpret because the age spectra are often disturbed and relatively few plateau ages can therefore be defined. Additional analytical and inter-

pretation difficulties arise from the fine-grained nature of the clay minerals dated (Fig. 3g), causing partial radiogenic argon loss and $^{39}Ar_K$ recoil, which would explain, to a degree, the disturbed age spectra. Clay minerals have relatively low argon retention (due to their large specific surface and low crystallinity; McDougall and Harrison 1999), which explains the great susceptibility of the material dated to partial resetting of its argon isotopic system, leading to disturbed age spectra. This resetting results in the presence, in most samples, of discrete isotopic reservoirs with distinct argon composition, each reflecting the age of the corresponding fluid circulation or thermal event that produced this partial resetting. One technique permitting the extraction of age information from disturbed age spectra is the Kernel density analysis (e.g., Alexandre et al. 2004) based on the ages of all individual steps and their error margins. This analysis relies on the hypothesis that the phases dated contain several sites with different isotopic compositions, each of which retains different, but geologically meaningful, age information. This is in agreement with age spectra containing two pseudo-plateau ages that are frequently observed, indicating that two distinct ages have been recorded corresponding to two sites with distinct isotopic compositions and argon retention characteristics. The Kernel technique, based on cumulating of the probabilities of the individual steps over the age span of interest assuming Gaussian distribution of the individual probabilities (detailed description of the method, including formulas, is available in Alexandre et al. 2004), permits extraction, visualization, and utilization of age information from the disturbed age spectra and makes comparison of age information from different minerals possible.

Samples analyzed

For U/Pb analyses, massive uraninite from the McArthur River basement-hosted ore body and disseminated uraninite from the Virgin River and Southwest sandstone-hosted prospects were analyzed. The massive uraninite crystals from McArthur River are often euhedral or colloform, with heterogeneous reflectance when observed in reflected light. The lower reflectivity zones along the edge of the grain or along fractures inside the grain correspond to altered uraninite (Alexandre and Kyser 2005). Zones that appear to be homogeneous in reflected light commonly reveal the presence of areas with variable brightness when observed by SEM. These low-reflectivity areas have irregular shapes, mostly independent of the morphology of the grain, and vary in size from a few to nearly 100 μm. The disseminated uraninite grains from the Virgin River prospect and the uraniferous bitumen globules from the Southwest prospect rarely exceed 150 μm across. All grains reveal heterogeneous reflectivity, with predominantly darker areas that correspond to altered uraninite. In most cases, micron-sized grains of galena, precipitated from radiogenic lead, are present.

For $^{40}Ar/^{39}Ar$ dating, six muscovite samples from the metamorphic host rock of the basement deposits in the east Athabasca and three biotite and one K-feldspar samples from the basement under the sandstone-hosted prospects in the west were analyzed to determine the age of the post-peak metamorphism cooling of the basement rocks. The age of the pre-ore alteration was determined using ten illite and eight chlorite samples from the pre-ore alteration of the basement-hosted deposits and 18 illite, four kaolinite, and three chlorite samples from the pre-ore alteration of the sandstone-hosted prospects. The mineralization age was determined using six illite samples from the syn-ore alteration of the basement-hosted deposits. In all cases, the clay minerals were analyzed by XRD and electron microprobe and only pure monomineral fractions were used. Samples with higher crystallinity, typically <0.4° $\Delta 2\theta$, were preferred. When possible, size fractions larger than 5 μm were used, and crystals smaller than 2 μm were systematically rejected to minimize problems of $^{39}Ar_K$ recoil. In the case of chlorite, electron microprobe analyses were performed on the pure clay separates and on thin sections, and only samples with potassium present (in our case, 0.08 to 0.27 wt% K_2O) were selected for $^{40}Ar/^{39}Ar$ dating.

Results

U/Pb dating of uraninite and uranium-rich bitumen

Uraninite from the massive ore zone at the McArthur River basement-hosted deposit have U/Pb isotopic compositions that define three distinct discordia lines and $^{207}Pb/^{206}Pb$ ages (Fig. 5a, Table 1). These include one group with an upper intercept age of 1,540±19 Ma (MSWD=0.75; average $^{207}Pb/^{206}Pb$ age=1,570±38 Ma), another with an upper intercept age of 1,247±19 Ma (MSWD=3.2; average $^{207}Pb/^{206}Pb$ age=1,251±49 Ma), and a third with an upper intercept age of 971±27 Ma (MSWD=2.3; average $^{207}Pb/^{206}Pb$ age=975±48 Ma; Fig. 5a). All lower intercepts are undistinguishable, at the present level of analytical uncertainty, from an age of 0 Ma (Fig. 5a), indicating significant modern radiogenic lead loss possibly produced by percolating oxidizing meteoric waters (Alexandre et al. 2005). Given the propensity of the U/Pb isotopic system to be reset in uraninite (Fayek and Kyser 2000; Alexandre and Kyser 2005), the highest age is interpreted as a minimum estimate of the initial crystallization age of the uraninite at McArthur River, whereas the two lower ages correspond to recrystallizations of uraninite (Alexandre and Kyser 2005). A few inversely discordant data are observed, which is

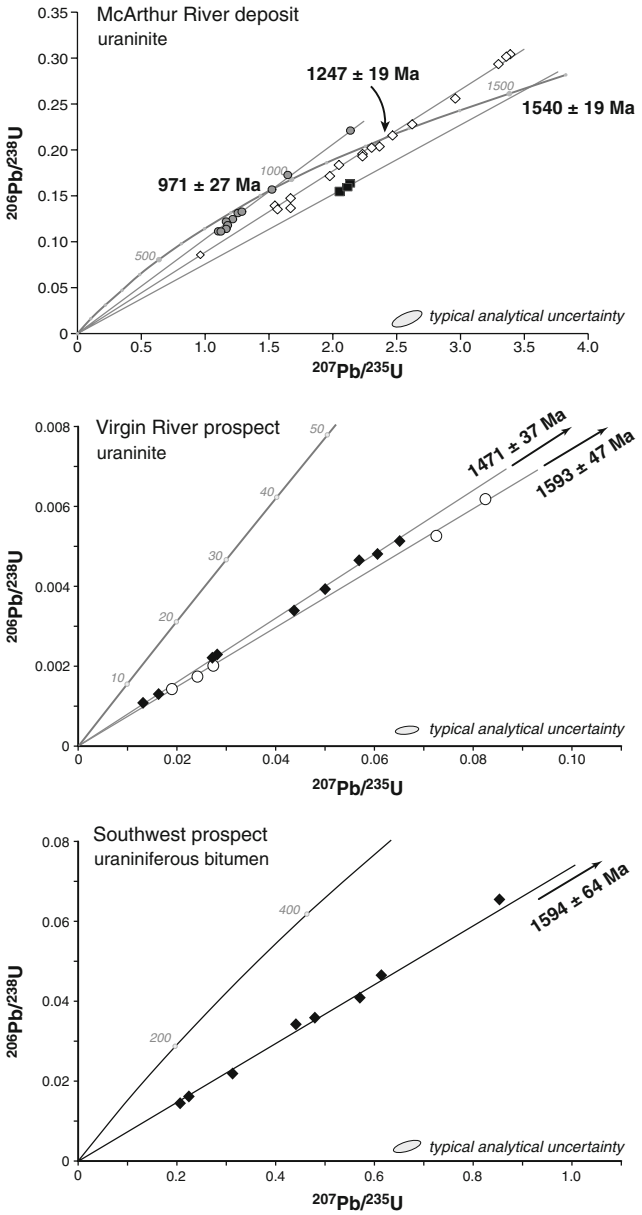

Fig. 5 Concordia diagrams showing the results of the U/Pb dating of the uranium rich minerals from the studied mineralizations. The upper intercept ages, as calculated using Isoplot, are indicated

probably explained by the presence of sub-micrometer-sized galena grains, the lead of which is produced by the radioactive disintegration of uranium in adjacent uraninite (Fig 4a; Alexandre and Kyser 2005).

Disseminated uraninite analyses from Virgin River sandstone-hosted mineralization are strongly discordant, with very low Pb/U ratios indicating severe Pb loss (Fig. 5b). However, the $^{207}Pb/^{206}Pb$ ratios distinguish two populations corresponding to two U/Pb discordia lines with upper intercepts of 1,593±47 Ma (MSWD=3.3) and 1,471±37 Ma (MSWD=3.9) and lower intercepts undistinguishable, within analytical uncertainty, from an age of 0 Ma, indicating recent lead loss. The average $^{207}Pb/^{206}Pb$ ages of the two groups are 1,593±38 Ma and 1,445±46 Ma, respectively. The higher age is interpreted as initial crystallization age and the lower a result of uraninite alteration.

The results of the U/Pb analyses of uraniferous bitumen from the sandstone-hosted mineralization at Southwest (Table 1) are very similar to those from Virgin River in that the Pb/U ratios are very low, indicating strong radiogenic Pb loss (Fig. 5c). However, the data define a discordia with upper intercept of 1,594±64 Ma (MSWD=1.8), the lower intercept being undistinguishable from the origin. The average $^{207}Pb/^{206}Pb$ age of 1,593±52 Ma is identical, within the analytical uncertainty, to the upper intercept age.

The initial crystallization ages obtained in these distinct areas are identical within the analytical uncertainty. The highest upper intercept and $^{207}Pb/^{206}Pb$ ages are close to the age of 1,598±25 Ma obtained by U/Pb ion-probe dating of uraninite from one of the sandstone-hosted uraninite orebodies of the McArthur River deposit just above the basement-hosted ore body studied here (Fayek, personal communication).

$^{40}Ar/^{39}Ar$ dating

Muscovite samples from unaltered host rocks of the basement-hosted deposits at McArthur River and Dawn Lake have plateau and pseudo-plateau $^{40}Ar/^{39}Ar$ ages that vary from 1,709 to 1,753 Ma (Table 2), with a weighted average of 1,731±18 Ma. All samples show limited degree of superficial $^{40}Ar^*$ loss (Fig. 6), but this does not affect the validity of the ages.

Three biotite and one potassic feldspar samples from a slightly altered deformed granitoid in the metamorphic basement under the sandstone-hosted Virgin River prospect give relatively disturbed spectra, with only two samples having plateau ages (biotite samples VR03-926 and VR03-949). For the two other samples, average ages on the relatively flat portion of the spectrum are calculated. The plateau ages and the average ages vary between 1,680 and 1,760 Ma and form two distinct groups at ca 1,685 and 1,750 Ma (Fig. 6).

Seven samples of pre-ore alteration illite were dated, one from the Rabbit Lake deposit and three for the McArthur River and the Dawn Lake deposits. The analyses give disturbed age spectra that are either bell-shaped or indicate strong superficial $^{40}Ar^*$ loss (Fig. 7). In most cases, it is possible to define pseudo-plateau ages on 30 to 50% of the gases released (Table 2), and for other samples, the average age on a relatively flat portion of the spectrum is given. The age of the oldest step in bell-shaped spectra is often interpreted as a minimum estimate of the crystallization age (e.g., McDougall and Harrison 1999). The proposed

Table 1 Analytical data of the U–Pb LA-HR-ICP-MS analyses of uranium-rich minerals in the studied areas

		Corrected ratios						Calculated ages (Ma)					
Sample analytical point	$^{206}Pb/^{204}Pb$ ×1,000	$^{207}Pb/^{206}Pb$	±	$^{207}Pb/^{235}U$	±	$^{206}Pb/^{238}U$	±	$^{207}Pb/^{206}Pb$	±	$^{207}Pb/^{235}U$	±	$^{206}Pb/^{238}U$	±
McArthur River (uraninite)													
6	176	0.0970	0.0039	2.1394	0.0856	0.1642	0.0066	1,568	63	1,162	46	980	39
9		0.0963	0.0039	2.0564	0.0823	0.1545	0.0062	1,553	62	1,134	45	926	37
17	5,507	0.0982	0.0039	2.1119	0.0845	0.1600	0.0064	1,590	64	1,153	46	957	38
26	29	0.0820	0.0033	1.6688	0.0668	0.1482	0.0059	1,245	50	997	40	891	36
16	23	0.0815	0.0033	1.5440	0.0618	0.1396	0.0056	1,232	49	948	38	842	34
14	32	0.0820	0.0033	2.3626	0.0945	0.2043	0.0082	1,246	50	1,231	49	1199	48
12a	231	0.0833	0.0033	2.6151	0.1046	0.2279	0.0091	1,277	51	1,305	52	1323	53
11a	518	0.0835	0.0033	2.4661	0.0986	0.2164	0.0087	1,282	51	1,262	50	1263	51
10	135	0.0822	0.0033	1.9691	0.0788	0.1721	0.0069	1,251	50	1,105	44	1023	41
9a	109	0.0824	0.0033	2.3014	0.0921	0.2034	0.0081	1,256	50	1,213	49	1194	48
6	858	0.0815	0.0033	2.0471	0.0819	0.1848	0.0074	1,234	49	1,131	45	1093	44
9b	27	0.0818	0.0033	2.2288	0.0892	0.1967	0.0079	1,241	50	1,190	48	1158	46
8	32	0.0820	0.0033	2.2342	0.0894	0.1941	0.0078	1,246	50	1,192	48	1144	46
7	43	0.0838	0.0034	2.9558	0.1182	0.2565	0.0103	1,288	52	1,396	56	1472	59
15	232	0.0816	0.0033	3.2913	0.1317	0.2950	0.0118	1,237	49	1,479	59	1666	67
14a	30	0.0843	0.0034	1.5629	0.0625	0.1364	0.0055	1,300	52	956	38	824	33
14b	333	0.0799	0.0032	3.3854	0.1354	0.3055	0.0122	1,194	48	1,501	60	1718	69
13a	217	0.0799	0.0032	3.3653	0.1346	0.3026	0.0121	1,194	48	1,496	60	1704	68
13b	29	0.0879	0.0035	1.6681	0.0667	0.1381	0.0055	1,380	55	996	40	834	33
13c	35	0.0785	0.0031	0.9564	0.0383	0.0868	0.0035	1,158	46	681	27	537	21
9c	66	0.0752	0.0030	1.1638	0.0466	0.1133	0.0045	1,074	43	784	31	692	28
9d	28	0.0735	0.0029	1.1175	0.0447	0.1115	0.0045	1,028	41	762	30	681	27
19	43	0.0730	0.0029	1.2985	0.0519	0.1313	0.0053	1,014	41	845	34	795	32
23	84	0.0708	0.0028	1.5329	0.0613	0.1556	0.0062	954	38	944	38	932	37
22	30	0.0713	0.0029	1.1738	0.0470	0.1186	0.0047	967	39	788	32	723	29
21	51	0.0702	0.0028	1.2715	0.0509	0.1307	0.0052	935	37	833	33	792	32
18	53	0.0716	0.0029	1.2240	0.0490	0.1232	0.0049	975	39	812	32	749	30
12b	17	0.0716	0.0029	1.0962	0.0438	0.1111	0.0044	975	39	752	30	679	27
4	35	0.0695	0.0028	1.6509	0.0660	0.1725	0.0069	912	36	990	40	1026	41
8	50	0.0697	0.0028	1.1760	0.0470	0.1220	0.0049	920	37	789	32	742	30
11b	52	0.0715	0.0029	2.1456	0.0858	0.2198	0.0088	971	39	1164	47	1281	51
Virgin River (uraninite)													
1	1.25	0.0875	0.0031	0.0131	0.0005	0.0011	0.0000	1,371	55	13	1	7	0
3	0.21	0.0903	0.0032	0.0163	0.0006	0.0013	0.0000	1,432	57	16	1	8	0
4		0.0886	0.0031	0.0570	0.0020	0.0047	0.0002	1,396	56	56	2	30	1
9	0.40	0.0889	0.0031	0.0282	0.0010	0.0023	0.0001	1,401	56	28	1	15	1
10	0.54	0.0920	0.0032	0.0649	0.0023	0.0051	0.0002	1,468	59	64	3	33	1
13		0.0922	0.0032	0.0499	0.0017	0.0039	0.0001	1,472	59	49	2	25	1
14	30.31	0.0914	0.0032	0.0605	0.0021	0.0048	0.0002	1,455	58	60	2	31	1

17		0.0933	0.0033	0.0437	0.0015	0.0034	0.0001	1,493	60	43	2	22	1
18		0.0889	0.0031	0.0272	0.0010	0.0022	0.0001	1,402	56	27	1	14	1
5		0.1001	0.0035	0.0728	0.0025	0.0053	0.0002	1,625	65	71	3	34	1
6		0.0963	0.0034	0.0190	0.0007	0.0014	0.0001	1,553	62	19	1	9	0
15		0.0967	0.0034	0.0823	0.0029	0.0062	0.0002	1,562	62	80	3	40	2
19		0.1008	0.0035	0.0242	0.0008	0.0017	0.0001	1,638	66	24	1	11	0
21	0.09	0.0979	0.0034	0.0273	0.0010	0.0020	0.0001	1,585	63	27	1	13	1
Southwest (uraniferous bitumen)													
6	1.07	0.0955	0.0029	0.6139	0.0184	0.0466	0.0014	1,538	62	486	19	294	12
10	0.55	0.0945	0.0028	0.8539	0.0256	0.0655	0.0020	1,518	61	627	25	409	16
Line 2	0.56	0.0966	0.0029	0.4793	0.0144	0.0360	0.0011	1,559	62	398	16	228	9
Line 4	0.65	0.0931	0.0028	0.4417	0.0132	0.0344	0.0010	1,490	60	371	15	218	9
5		0.1006	0.0030	0.2242	0.0067	0.0162	0.0005	1,635	65	205	8	103	4
8	0.78	0.1036	0.0031	0.2061	0.0062	0.0144	0.0004	1,689	68	190	8	92	4
11	1.00	0.1028	0.0031	0.3125	0.0094	0.0220	0.0007	1,676	67	276	11	141	6
Line 1	0.62	0.1010	0.0030	0.5711	0.0171	0.0410	0.0012	1,643	66	459	18	259	10

ages, including pseudo-plateau, averages on flat portions, and oldest step ages, vary from 1,330±90 Ma to 1,671± 7 Ma and can be divided into three different age groups: (1) at ca 1,650 to 1,670 Ma, (2) at ca 1,600 Ma, and (3) ca 1,500 to 1,530 Ma (Table 2). The first of these ages is interpreted as the initial crystallization age of the pre-ore illite, while the other ages correspond to perturbations of the isotopic system of the minerals dated.

Four samples of pre-ore alteration chlorite were also analyzed, three from the Rabbit Lake and one from the Dawn Lake deposit, with duplicate analyses for three of them. Most of the analyses provide strongly disturbed age spectra and pseudo-plateau ages on 50 to 80% of the released gases are defined in only in a few cases (Fig. 7). The pseudo-plateau ages and the oldest step ages vary from 1,355±40 Ma to 1,617±136 Ma (Table 2). The majority of ages range between ca 1,300 and 1,500 Ma.

Syn-ore illite samples from the Dawn Lake and McArthur River basement-hosted deposits provide disturbed age spectra, indicating moderate $^{40}Ar^{*}$ loss (Fig. 8). Pseudo-plateau ages were defined on 20 to 60% of the gas released, and average ages are defined on relatively flat portions of a spectrum. The proposed ages vary from 1,277 Ma (sample 11A-112-150) to 1,583 Ma (sample 11B-711-142; Fig. 8). Examination of the age spectra does not reveal the presence of obvious age groups, but pseudo-plateau ages of ca 1,530 to 1,585 Ma are visible in almost all samples (Fig. 8).

Argon analyses of pre-ore alteration illite, chlorite, and kaolinite from the sandstone-hosted areas provide two types of age spectra, one with flat spectra and good plateau ages and one having bell-shaped spectra on which pseudo-plateau ages can be defined (Fig. 9). In some cases, the spectra were disturbed precluding the definition of a pseudo-plateau, in which case, the age of the oldest step was taken. The oldest step ages vary from 851±37 to 1,531± 7 Ma, whereas the plateau and pseudo-plateau ages vary less, from 1,073±6 to 1,460±8 Ma (Table 2). Most of the ages are higher than 1,300 Ma (Table 2), with a large cluster of ages at ca 1,410 to 1,440 Ma and one well-defined plateau age of 1,460±8 Ma (Fig. 9).

Distribution of the $^{40}Ar/^{39}Ar$ ages

The Kernel statistical analysis permits the definition of major ages for the various sample groups dated presented above, each peak in the cumulative probability diagram corresponding to a discrete age (Fig. 10). For each group, the first peak is interpreted to correspond to the initial crystallization age or to the oldest preserved age, whereas all subsequent peaks correspond to perturbations of the argon isotopic system of the phases analyzed.

The first peak for samples from the basement rocks throughout the Athabasca Basin is ca 1,740 Ma, with an

Table 2 Result of the $^{40}Ar/^{39}Ar$ dating of various metamorphic and intrusive the host rocks and alteration minerals from the alteration halo in the basement-hosted and sandstone-hosted uranium deposits and prospects in Athabasca Basin

Samples	Mineral	Deposit	Plateau or pseudo-plateau age (Ma)	Length of plateau (% of released gas)	Oldest step age (Ma)
Basement-hosted deposits: metamorphic host rock					
8220-387-55a	Muscovite	McArthur River	1,740±8	99	
8180-231-100	Muscovite	McArthur River	1,726±8	93	
8270-201-46	Muscovite	McArthur River	1,747±7	96	
8220-267-52	Muscovite	McArthur River	1,753±8	52	
11A-208-176	Muscovite	Dawn Lake	1,712±9	97	
11B-605-132	Muscovite	Dawn Lake	1,709±16	66	
Basement-hosted deposits: pre-ore alteration					
11A-208-150	Illite	Dawn Lake	1,505±10	34	
11B-605-138	Illite	Dawn Lake	1,330±90	37	
8220-267-52	Illite	McArthur River	1,595±48	50	
11B-605-1057	Illite	Dawn Lake	–	–	1,528±8
593-65.5	Illite	McArthur River	1,669±4	45	
593-65.5 duplicate	Illite	McArthur River	1,666±6	31	
329-497.5	Illite	McArthur River	1,671±7	29	
329-497.5 duplicate	Illite	McArthur River	–	–	1,676±19
7-124-189	Illite	Rabbit Lake	1,649±18	48	
7-124-150-a	Chorite	Rabbit Lake	–	–	
7-124-150-a duplicate	Chorite	Rabbit Lake	1,355±40	58	
7-124-150-b	Chorite	Rabbit Lake	1,476±159	78	
7-124-150-b duplicate	Chorite	Rabbit Lake	1,553±15	51	
7-124-150-c	Chorite	Rabbit Lake	1,514±65	84	
11B-605-138	Chorite	Dawn Lake	–	–	1,617±136
11B-605-138 duplicate	Chorite	Dawn Lake	–	–	1,545±50
Basement-hosted deposits: syn-ore alteration					
11A-112-150	Illite	Dawn Lake	1,277±12	24	
11A-112-150 duplicate	Illite	Dawn Lake	1,298±28	39	
11B-711-142	Illite	Dawn Lake	1,583±17	39	
8220-387-55	Illite	McArthur River	1,533±13	56	
11A-208-150	Illite	Dawn Lake	1,513±14	27	
8220-265-28	Illite	McArthur River	1,433±41	20	
Sandstone-hosted prospects: basement rocks					
VR03-949	Biotite	Virgin River	1,760±4	78	
VR03-949	K-feldspar	Virgin River	1,711±12	44	
VR03-926	Biotite	Virgin River	1,738±5	49	
VR03-931	Biotite	Virgin River	1,677±10	33	
Sandstone-hosted prospects: pre-ore alteration					
MAC214-303	Illite	McArthur River	1,366±7	34	
MAC223-261	Illite	McArthur River	1,340±4	100	
HK15-75	Illite	Hook Lake	1,435±4	46	
VR01-1112	Illite	VR01	1,460±8	81	
VR01-754	Illite	VR01	1,403±4	69	
VR01-901	Illite	VR01	1,415±8	63	
VR05-760.5, 2–5 μm	Illite	Virgin River	1,355±5	56	
VR05-760.5, 5–10 μm	Illite	Virgin River	1,351±6	37	
VR05-760.5, > 10 μm	Illite	Virgin River	1,333±6	37	
VR05-693.5, 2–5 μm	Illite	Virgin River	1,396±6	53	
VR05-693.5, 5–10 μm	Illite	Virgin River	–	–	1,379±5
VR05-693.5, > 10 μm	Illite	Virgin River	1,392±7	48	
VR15-647.5	Illite	Virgin River	1,427±6	69	
VR03-763	Illite	Virgin River	–	–	1,531±7
VR13-750	Illite	Virgin River	1,409±5	47	
VR15-281	Illite	Virgin River	1,435±6	42	
VR13-827	Illite	Virgin River	–	–	1,320±5
VR13-652	Illite	Virgin River	1,412±6	61	
SW03-369	Kaolinite	Southwest	1,224±47	37	
VR12-734	Kaolinite	Virgin River	–	–	938±41

Table 2 (continued)

Samples	Mineral	Deposit	Plateau or pseudo-plateau age (Ma)	Length of plateau (% of released gas)	Oldest step age (Ma)
VR12-734	Kaolinite	Virgin River	–	–	851±37
VR12-808.5	Kaolinite	Virgin River	–	–	583±51
VR04-807.5	Chlorite	Virgin River	1,073±6	33	
VR04-821	Chlorite	Virgin River	–	–	1,221±16
SW12-341	Chlorite	Southwest	–	–	1,253±8

age of 1,732±10 Ma for the muscovite samples in the basement-hosted deposits in the east and an age of 1,743±10 Ma for the biotite and hornblende samples in the west (Fig. 10). The basement rocks in the west of the basin, under the sandstone-hosted mineralizations, also have a well-marked peak at 1,692±11 Ma and another at 1,625±4 Ma (Fig. 10). All basement samples record minor perturbation events at ca 1,530 Ma and ca 1,410 Ma expressed as small peaks (Fig. 10).

The pre-ore alteration minerals in the basement have four major and well-defined peaks at 1,665±11 Ma, 1,597±11 Ma, 1,525±21 Ma, and 1,399±1a Ma, as well as a few minor ones (Fig. 10). Pre-ore alteration minerals in the sandstone-hosted prospects have one large peak at 1,405±24 Ma, followed by two minor peaks at 1,339±11 Ma and 1,274±17 Ma, as well as a few smaller ones (Fig. 10). Finally, the first observable peak in syn-ore alteration minerals in the basement-hosted deposits is at 1,583±15 Ma, followed by three peaks at 1,527±15 Ma, 1,382±25 Ma, and 1,280±13 Ma (Fig. 10).

Discussion

Age of uraninite precipitation

Until recently, the unconformity-related uranium deposits in the Athabasca Basin were considered to have formed at ca 1,400 Ma (e.g., Baagsgard et al. 1984), but recent data indicated that they were older, as old as 1,521±8 Ma (McGill et al. 1993). Our data confirm this, with U/Pb ages of uraninite obtained in this study varying from 1,540±19 Ma at McArthur River to 1,594±64 Ma at Southwest. Further, the oldest syn-ore illites have a similar $^{40}Ar/^{39}Ar$ age of 1,583±17 Ma (Fig. 8), with the first peak in the cumulative probability diagram at 1,583±15 Ma (Fig. 10). The weighted average of all these ages, including the age of 1,598±25 Ma for the McArthur River sandstone-hosted deposit (Fayek, personal communication), is 1,588±15 Ma. Given that this age is very consistent in both sandstone- and basement-hosted deposits, it is very likely the age of the major uraninite formation event in the Athabasca Basin.

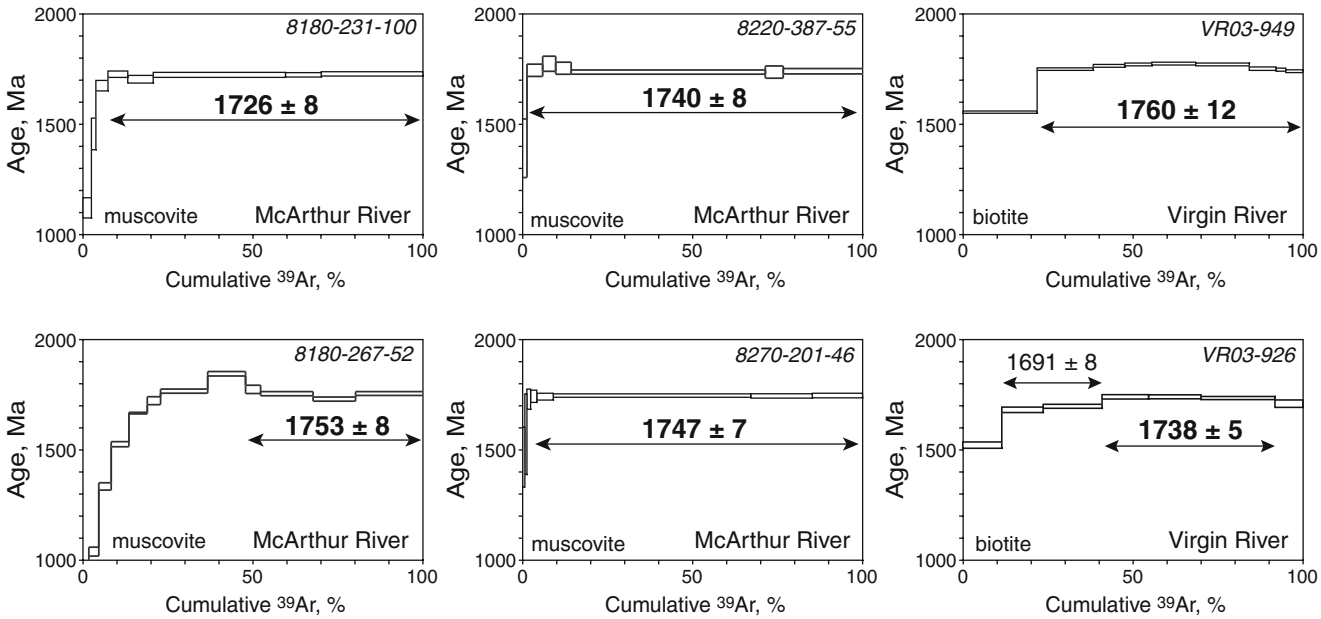

Fig. 6 Typical $^{40}Ar/^{39}Ar$ age spectra for the unaltered basement rocks from the basement-hosted deposit McArthur River and from the sediment-hosted mineralization Virgin River. Note that two steps from sample VR03-926 from Virgin river form a pseudo-plateau of ca 1,690 Ma, indicating that this sample has been disturbed by a subsequent fluid event of this age. All ages indicated are in Ma. Full analytical data in Appendix

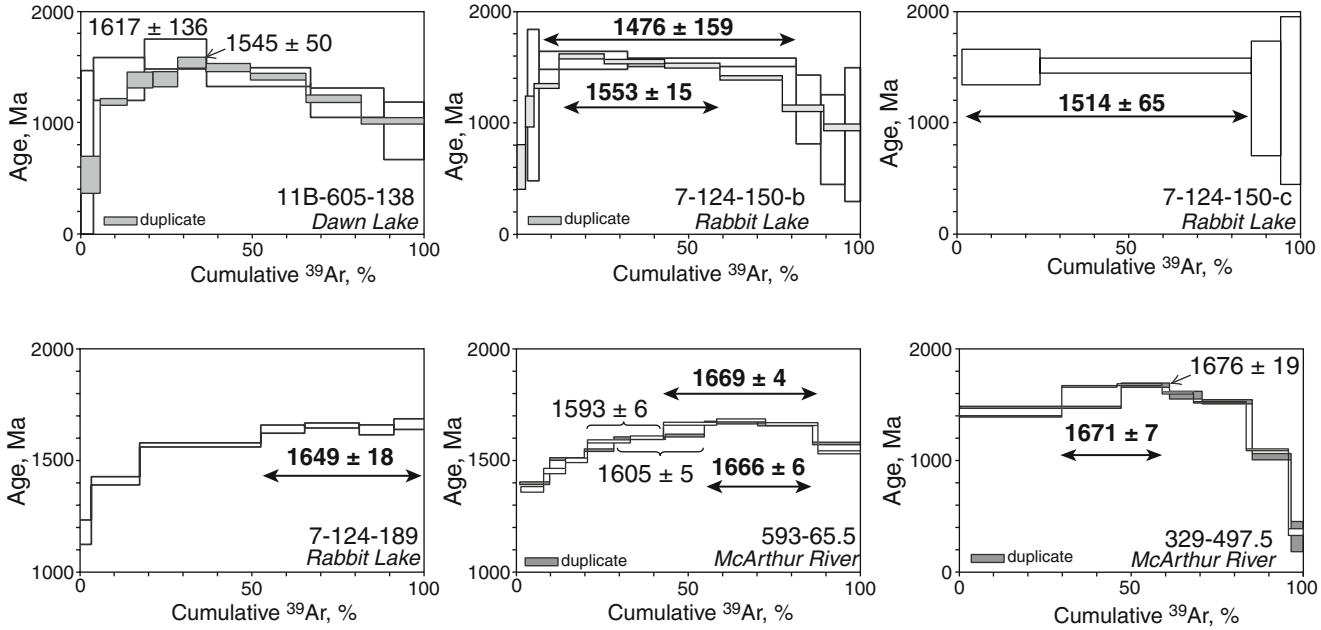

Fig. 7 Typical $^{40}Ar/^{39}Ar$ age spectra for pre-ore alteration in the basement-hosted deposits. The plateau ages are indicated in *bold*, while the pseudo-plateau ages and oldest step ages are given in *regular font*. Sample 593-65.5 from McArthur River retains a pseudo-plateau age at ca 1,600 Ma, indicative of a perturbation event of this age. All ages indicated are in Ma. Full analytical data in Appendix

Evolution of the basin and the deposits

The oldest age obtained by the $^{40}Ar/^{39}Ar$ method is 1,742± 25 Ma (weighted mean) obtained on minerals from the metamorphic and intrusive rocks in the basement of Athabasca Basin, both in the east and the west of the basin (Fig. 10). This age is similar to that of 1,720 to 1,735 Ma obtained by $^{40}Ar/^{39}Ar$ dating of micas and amphibole from basement rocks in the Trans-Hudson Orogen, which corresponds to rapid uplift of the domain to the east of the Athabasca Basin (Kyser et al. 2000). Thus, the basement rocks of the Athabasca Basin were also subjected to exhumation and post-peak metamorphism cooling at ca 1,730 Ma, at the end of the Trans-Hudson Orogeny. This represents a maximum age of the formation of the basin at this time (Fig. 11).

Formation of the basin was followed by basin-wide diagenetic alteration related to subsidence and burial of the sediments. The pre-ore alteration event, particularly visible in the basement-hosted deposits, is distinct from the early diagenetic alteration, but coeval with peak diagenesis of the basin fill (Fig. 4; Kyser et al. 2000). The age for the pre-ore alteration is given by the pre-ore alteration clay minerals in the basement-hosted deposits in the east at 1,665±11 Ma (Fig. 10) and by the perturbation registered by the basement minerals near the sandstone-hosted prospects in the west at 1,692±11 Ma (Fig. 10). Using all these data, the average age for the pre-ore alteration is 1,675±15 Ma (Fig. 11), and is ca 65 Ma later that of the formation of the basin. The pre-ore alteration clay minerals in the sandstone-hosted prospects in the west have an oldest age of 1,405±24 Ma (Fig. 10), much less than expected from the paragenesis or

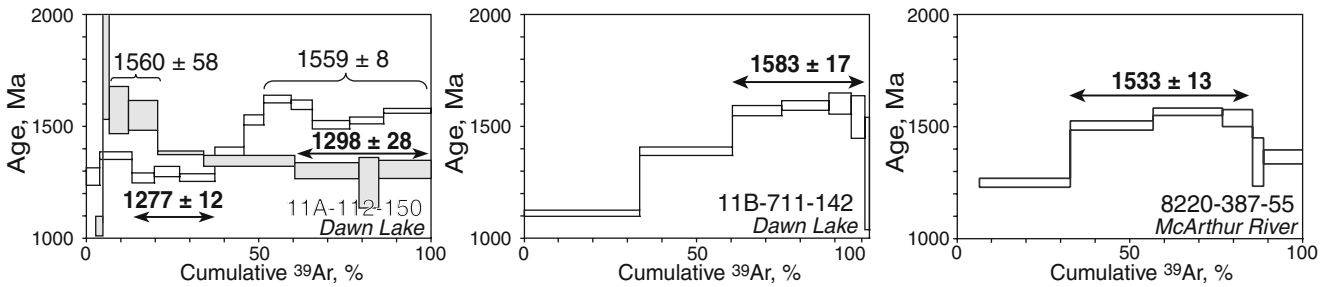

Fig. 8 Typical $^{40}Ar/^{39}Ar$ age spectra for syn-ore illite in the basement-hosted deposits. The plateau ages are given in *bold*. Note that sample 11A-112-150 retains two distinct ages, one close to the initial crystallization at ca 1,560 Ma, the other indicating the perturbation related to the emplacement of the Mackenzie dykes at ca 1,270 Ma (LeCheminant and Heaman 1989). All ages indicated are in Ma. Full analytical data in Appendix

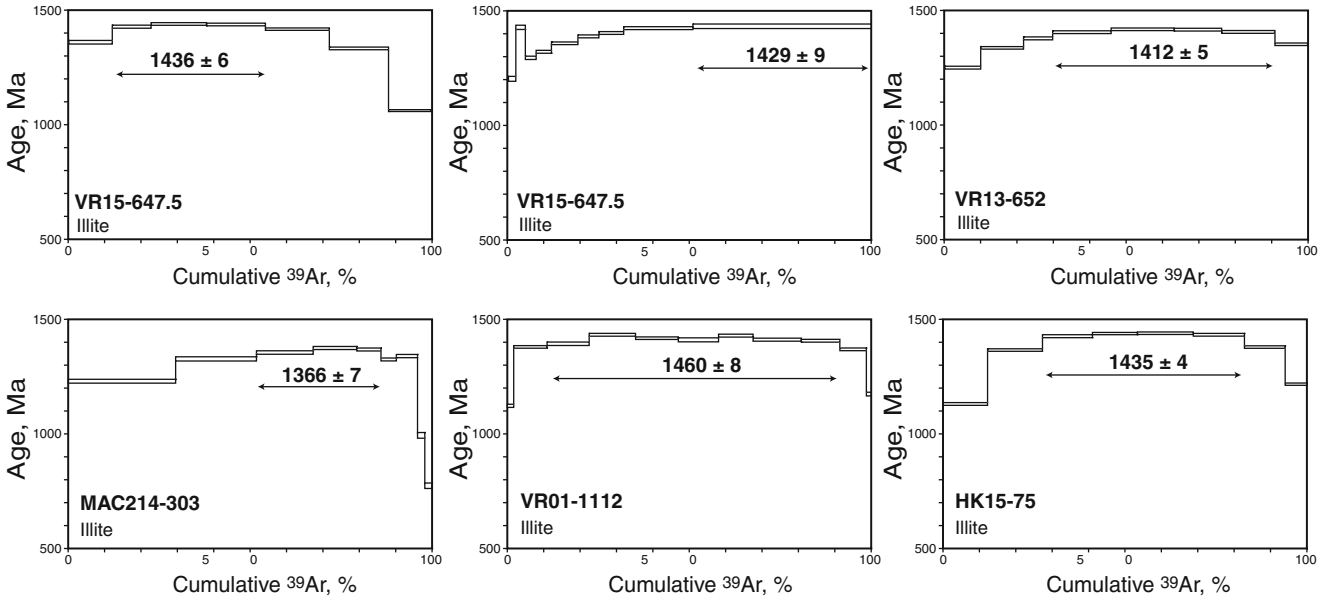

Fig. 9 Typical $^{40}Ar/^{39}Ar$ age spectra for pre-ore alteration in the sediment-hosted prospects. All ages indicated are in Ma. Full analytical data in Appendix

the U/Pb mineralization age of uraninite of ca 1,590 M (Fig. 5b and c). This is most likely the result of the larger amounts of fluids present in the sandstones relative to the basement, causing continuous alterations and argon loss. Thus, the oldest age recorded by the pre-ore clay minerals at ca 1,405 Ma (Fig. 10) indicates the time at which the fluid systems in this part the basin became a closed system, rather the initial crystallization age.

Precipitation of uraninite at ca 1,590 Ma followed the pre-ore alteration in both the basement- and the sandstone-hosted mineralizations (Fig. 11). The ore-formation event has the same age (ca 1,590 Ma) as the tectonic reactivation of the Cheyenne Belt in southern Wyoming by the Battle Lake fault zone (BLFZ; 1.62 to 1.59 Ga; Duebendorfer et al. 2006), which may have provided the trigger for basin-wide uraninite precipitation. This was followed by a series of post-ore events (Fig. 4), the fluid circulations related to each of which perturbed both the $^{40}Ar/^{39}Ar$ and U/Pb isotopic systems of clay minerals, biotite, potassic feldspar, and uraninite. All phases, using either $^{40}Ar/^{39}Ar$ or U/Pb methods, record similar perturbation ages. The first of those perturbation ages is ca 1,525 Ma and affects all phases dated by the $^{40}Ar/^{39}Ar$ method (Fig. 10). This perturbation corresponds to the Mazatzal Orogeny in the present-day southwest USA and north Mexico (Romano et al. 2000; Medaris et al. 2003). An age of ca 1,470 Ma is recorded by the uraninite from Virgin River (Fig. 5b); it is not clear to which event this age corresponds. The next perturbation event at ca 1,400 Ma affected all phases dated by the $^{40}Ar/^{39}Ar$ method (Fig. 10) and corresponds to the Berthoud Orogeny in present-day southwest USA (Nyman et al. 1994; Sims and Stein 2001). The perturbation age of ca 1,275 Ma (Fig. 10), recorded by the argon systems of all clay minerals and by the uraninite at McArthur River, corresponds very well to the emplacement age of the McKenzie Mafic Dyke swarms that transect the basin at 1,267±2 Ma (LeCheminant and Heaman 1989). Several ages of ca 1,150 to 1,050 Ma (Fig. 10) correspond to the Grenvillian Orogeny (Hoffman 1990; Mosher 1996), whereas the ages of 1,000–950 to 850 Ma (Fig. 5a, Fig. 10) could be related to the assemblage and breakup of Rodinia (Mayers et al. 1996; Condie 2001).

Integration of the deposit formation in the evolution of the basin

From a geochronological point of view, the events related to the pre-ore alteration occurred ca 65 Ma after the basin began to form at ca 1,740 Ma (Fig. 11). Ore formation occurred at ca 1,590 Ma, that is, ca 85 Ma after pre-ore alteration (Fig. 11). The data presented here seem to suggest that these events did not follow a continuous evolution, but occurred in distinct stages. Furthermore, the pre-ore as well as the syn-ore events occurred at the same time throughout the basin, and are observed in both basement- and sandstone-hosted mineralization (Fig. 11). Thus, ore formation results from specific events, the cause of which appears to be external to the evolution of the Athabasca Basin, in particular far-field tectonic events occurring on the same continent. This is substantiated by the timing of post-ore perturbations that occurred at the

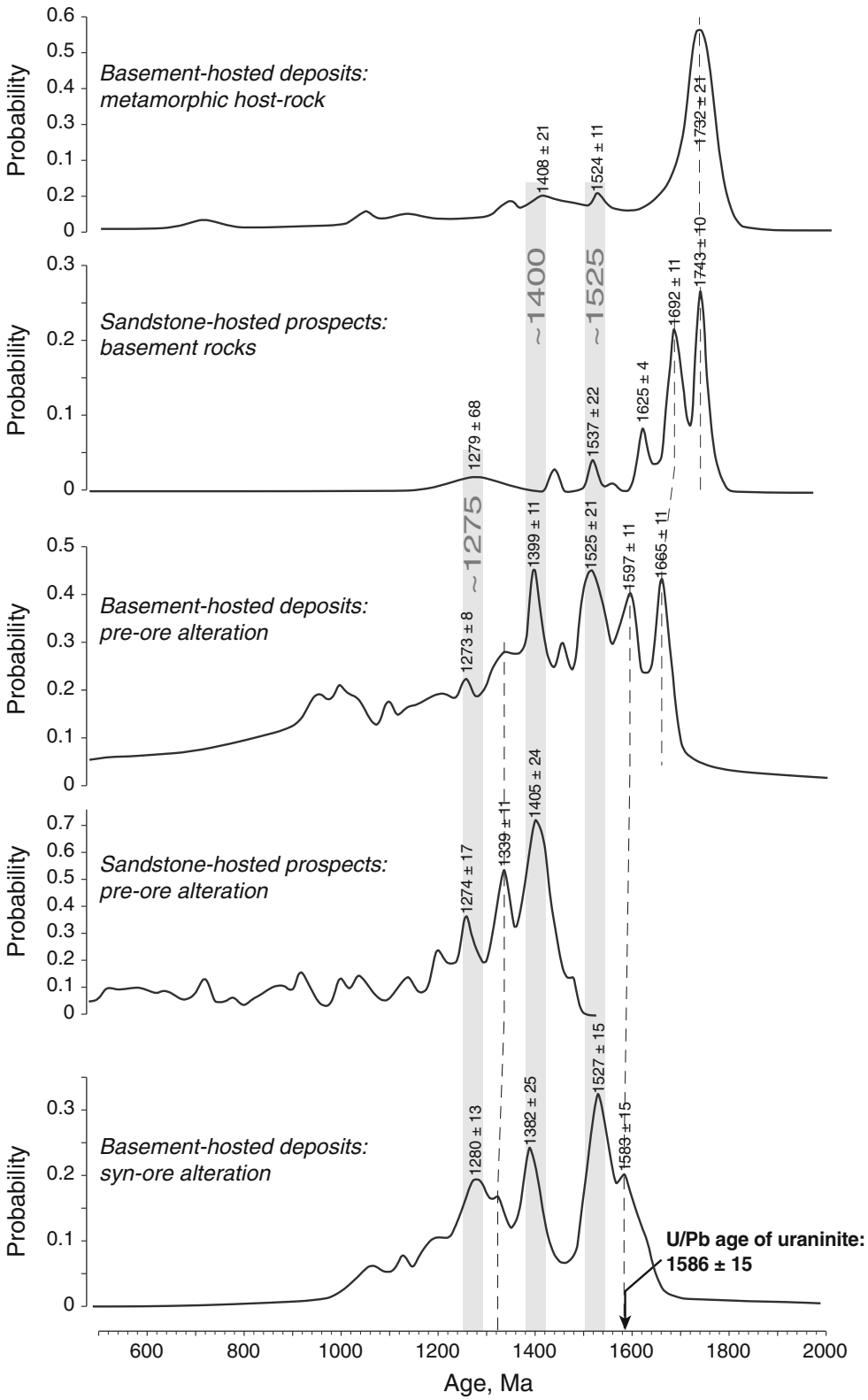

Fig. 10 Cumulative probability diagrams for all $^{40}Ar/^{39}Ar$ analyses calculated using the individual steps ages and error margins from the analytical data given in Appendix, organized by groups of dated samples, as indicated. The *gray bands* show the major perturbation events that affected all phases dated, corresponding to the end of the Mazatzal Orogeny (ca 1,525 Ma), the Bertoud Origeny (ca 1,400 Ma), and the emplacement of the Mackenzie dykes (ca 1,275 Ma). The ages of the individual peaks are indicated

same time throughout the basin, and in both the basement- and sandstone-hosted mineralization, and which have the same ages as well identified orogenies (Fig. 11). Although the basin fill most likely provided the source of most of the uranium via accessory detrital minerals and the fluids needed for the mobilization and transport of uranium, whereas the basement rocks provided structural and chemical traps needed to precipitate the

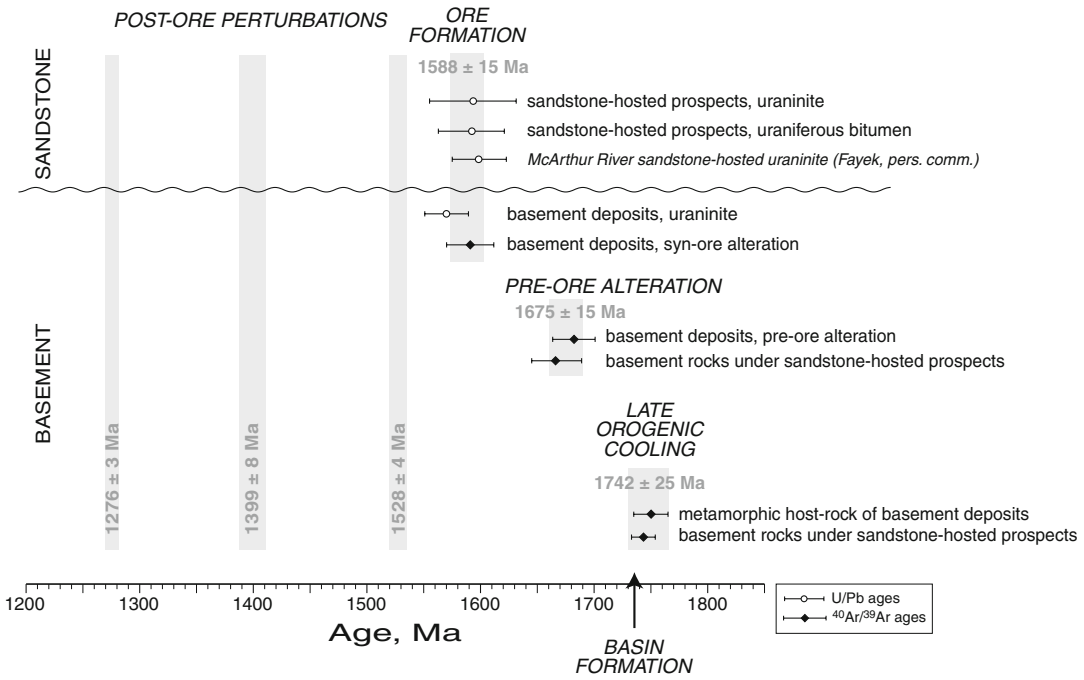

Fig. 11 Simplified reconstruction of the evolution of the Athabasca Basin and the unconformity-type uranium deposits in it, using the dating from this work and the ages from the cumulative probability diagrams in Fig. 10. The ages from the basement deposits are separated from those from the sandstone prospects by a *line* indicating unconformity. See text for detail

uraninite (e.g., Kotzer and Kyser 1995), the timing of events such as the pre-ore alteration and the uraninite precipitation were controlled primarily by events external to the Athabasca Basin.

Significance of the pre-ore events

The period between basin formation at ca 1,730 Ma and ore precipitation at ca 1,590 Ma is of particular interest and importance because it is during this time that most of the necessary conditions for the formation of uranium deposits were fulfilled. These critical conditions include:

(1) Leaching of uranium from the uranium-rich accessory minerals in the sandstones, such as apatite, monazite, and zircon, by oxidizing basin fluids and thus mobilizing it and thus making it available for uranium mineralization (Kotzer and Kyser 1995; Fayek and Kyser 1997);
(2) Pre-ore alteration, such as the early diagenetic silicification in the sandstones leading to compartmenting of the sedimentary sequence to aquitards and aquifers and, thus, channeling the fluid flow in the basin (Hiatt et al. 2001);
(3) Formation of structural traps, such as the intensely fractured thrust fault zones in the basement and the sandstones, which result from the reactivation of pre-Athabasca basement structures;
(4) Formation of chemical trap, such as the chlorite alteration zone, which acted as a strong reductant causing, jointly with graphite, uranium reduction and precipitation as uraninite (Alexandre et al. 2004).

Therefore, the pre-ore events in the period between ca 1,730 and 1,590 Ma are of paramount importance for the understanding of the genesis of unconformity-related uranium deposits in the Athabasca Basin. The subsequent post-ore events, from ca 1,590 Ma onwards, are important primarily from point of view of preservation of uraninite mineralizations and uranium remobilization.

Summary

Unconformity-related uranium mineralization in the Athabasca Basin formed at ca 1,590 Ma (Fig. 11), much earlier than what was previously proposed. Mineralization ages of ca 1,400 Ma obtained previously (e.g., Baagsgard et al. 1984; Carl et al. 1992; Philippe et al. 1993) correspond to periods when K/Ar and U/Pb systems were perturbed by fluid circulation initiated by far-field tectonic events, leading to uraninite recrystallization, radiogenic Pb loss, and partial uranium remobilization (Kotzer and Kyser 1995; Fayek and Kyser 1997; Fayek et al. 2002; Alexandre and Kyser 2005); they are not ages of initial mineralization. However, deposits formation is not coincident with the basin initiation or with pre-ore alteration events, but follows them by ca 140 and 85 Ma, respectively (Fig. 11). Major

ore-related events in the Athabasca Basin did not follow a continuous evolution, but proceeded by distinct stages at particular times. This means that these events reflect the influence of large-scale, probably continent-wide, events that are external to the basin. The basin and the fluids it contained were affected by external events, particularly far-field orogenic and tectonic events such as the Mazatzal Orogeny, Bertoud Orogeny, the emplacement of the McKenzie dykes, the Grenville Orogen, and the assemblage and breakup of Rodinia. Further, the observed pre-ore alteration, ore, and post-ore events are all basin-wide events (Fig. 10), thus, emphasizing that mineralization is related to the evolution of the entire Athabasca Basin, which should be studied in its entirety and not as a series of disconnected local systems. The period between the formation of the basin at ca 1,730 Ma and uraninite precipitation at ca 1,590 Ma, is critical for formation of unconformity-related uranium deposits, and subsequent perturbation events are important for remobilizing and preserving the uranium deposits.

Acknowledgements This work benefited from financial contribution by the Natural Sciences and Engineering Research Council of Canada (NSERC) via Discovery, Major Facility Access and Collaborative Research and Development grants. Cameco Corp. is acknowledged for its financial support. Vladimir Sopuck, Ken Wasyliuk, and Dan Jiricka are thanked for their field support and constructive discussions. Two anonymous reviewers contributed to the overall quality of the paper by thorough, detailed, and constructive comments.

References

Alexandre P, Chalot-Prat F, Saintot A, Wijbrans J, Stephenson R, Wilson M, Kitchka A, Stovba S (2004) $^{40}Ar/^{39}Ar$ dating of magmatic activity in the Donbas foldbelt and the Scythian platform (Eastern European Craton). Tectonics 23(5):TC5002

Alexandre P, Kyser TK (2005) Effects of cationic substitutions and alteration of uraninite, and implications for the dating of uranium deposits. Can Mineral 43:1005–1017

Alexandre P, Kyser K, Polito PA, Sopuck V, Thomas D (2005) Alteration mineralogy and stable isotope geochemistry of Paleoproterozoic basement-hosted unconformity-type uranium deposits in the Athabasca Basin, Canada. Econ Geol 100(8): 1547–1563

Alexandre P, Kyser TK (2006) Geochemistry of uraniferous bitumen in the southwest Athabasca Basin, Saskatchewan, Canada. Econ Geol 101:1605–1612

Armstrong RL, Ramaekers P (1985) Sr isotopic study of the Helikian sediment and diabase dikes in the Athabasca Basin, northern Saskatchewan. Can J Earth Sci 22:399–407

Baagsgard H, Cumming GL, Worden JM (1984) U-Pb geochronology of minerals from the Midwest uranium deposit, northern Saskatchewan. Can J Earth Sci 21:642–648

Bray CJ, Spooner ETC, Longstaffe FJ (1988) Unconformity-related uranium mineralization, McClean Deposits, North Saskatchewan, Canada: hydrogen and oxygen isotope geochemistry: Can Mineral 26:249–268

Burwash RA, Baadsgaard H, Morton RD (1962) Precambrian K-Ar dates from the Western Canada sedimentary basin. J Geophys Res 67:1617–1623

Carl C, von Pechmann E, Hondorf A, Ruhmann G (1992) Mineralogy and U/Pb, Pb/Pb, and Sm/Nd geochronology of the Key Lake uranium deposit, Athabasca Basin, Saskatchewan, Canada. Can J Earth Sci 29:879–895

Chandler FW (1978) Geology of part of the Wollaston Lake fold belt, northern Wollaston Lake, Saskatchewan. Can Geol Surv Bull 277:57

Chipley D, Polito P, Kyser K (in press) Measurement of U–Pb ages of uraninite and davidite by laser ablation-HR-ICP-MS. Amer Miner (in press)

Condie KC (2001) Rodinia and continental growth. In: Divi RS, Yoshida M (eds) Tectonics and mineralization in the Arabian Shield and its extensions. Gondwana Res 4(2):154–155

Cumming GL, Kristic D (1992) The age of unconformity uranium mineralization in the Athabasca Basin, northern Saskatchewan. Can J Earth Sci 29:1623–1639

Dalrymple GB, Alexander EC, Lanphere MA, Kraker GP (1981) Irradiation of samples for $^{40}Ar/^{39}Ar$ dating using the Geological Survey TRIGA reactor. US Geological Survey Professional Paper 1176

Duebendorfer EM, Chamberlain KR, Heizler M (2006) Filling the North American Proterozoic tectonic gap: 1.6–1.59 Ga deformation and orogenesis in southern Wyoming, USA. J Geology 114: 19–42

Fayek M, Kyser K (1997) Characterization of multiple fluid-flow events and rare-earth-element mobility associated with the formation of unconformity-type uranium deposits in the Athabasca Basin, Saskatchewan. Can Mineral 35:627–658

Fayek M, Kyser K (2000) Low temperature oxygen isotopic fractionation in the uraninite-UO_3-CO_2-H_2O system. Geochim Cosmochim Acta 64:2185–2197

Fayek M, Kyser TK, Riciputi L (2002) U and Pb isotope analysis of uranium minerals by ion microprobe and the geochronology of the McArthur River and Sue Zone uranium deposits, Saskatchewan, Canada. Can Mineral 40:1553–1569

Finch RJ, Murakami T (1999) Systematics and paragenesis of uranium minerals. In: Burns PC, Finch RJ (eds), Uranium: mineralogy, geochemistry, and the environment. Mineralogical Society of America, Reviews in Mineralogy 38. Washington, USA

Hiatt E, Fayek M, Kyser K, Polito P (2001) The importance of early quartz cementation events in the evolution of aquifer properties of ancient sandstones; isotopic evidence from ion probe analysis of sandstones from the McArthur, Athabasca, and Thelon basins. Geological Society of America, 2001 annual meeting, Abstracts with Programs 33:74

Hoeve J, Sibbald TII (1978) Rabbit Lake uranium deposit. In: Dunn CE (ed) Uranium in Saskatchewan. Saskatchewan Geological Society Special Publication 3:475–484

Hoffman PF (1990) Behind the Grenville Orogen. Abstracts with Programs, Geological Society of America 22(2):24

Knipping HD (1974) The concepts of a supergene versus hypogene emplacement of uranium at Rabbit Lake, Saskatchewan, Canada. In: Formation of uranium ore deposits: International Atomic Energy Agency, Vienna, pp 531–548

Kotzer T, Kyser TK (1995) Petrogenesis of the Proterozoic Athabasca Basin, northern Saskatchewan, and its relation to diagenesis, hydrothermal uranium mineralization and paleohydrology. Chem Geol 120:45–89

Kyser K, Chipley D, Bukata A, Polito P, Fitzpatrick A, Alexandre P (2003) Application of laser ablation and high resolution ICPMS to the analysis of metal contents in tree rings, ages of uranium-rich minerals and Se content in sulphide ores. Can J Anal Sci Spectrosc 48(5):258–268

Kyser K, Hiatt E, Renac C, Durocher K, Holk G, Deckart K (2000) Diagenetic fluids in paleo- and meso-proterozoic sedimentary basins and their implications for long protracted fluid histories. In: Kyser TK (ed) Fluids and basin evolution. Mineralogical Association of Canada Short Course 28:225–262

LeCheminant AN, Heaman LM (1989) Mackenzie igneous events, Canada: middle Proterozoic hotspot magmatism associated with ocean opening. Earth Planet Sci Lett 96:38–48

Lee JKW, Onstott TC, Hanes JA (1990) An $^{40}Ar/^{39}Ar$ investigation of the contact effects of a dyke intrusion, Kapuskasing structural zone, Ontario. A comparison of laser microprobe and furnace extraction techniques. Contrib Mineral Petrol 105:87–105

Lewry JF, Sibbald TII (1977) Variation in lithology and tectonometamorphic relationships in the Precambrian basement of northern Saskatchewan. Can J Earth Sci 14:1453–1477

Lewry JF, Sibbald TII (1980) Thermotectonic evolution of the Churchill province in Northern Saskatchewan. Tectonophysics 68: 49–82

McDougall M, Harrison TM (1999) Geochronology and thermochronology by the $^{39}Ar/^{40}Ar$ method. Oxford University Press, Oxford

McGill BD, Marlat JL, Matthews RB, Sopuck VJ, Homeniuk LA, Hubregtse JJ (1993) The P2 North uranium deposit, Saskatchewan, Canada. Explor Min Geol 2(4):321–331

Mayers JS, Shaw RD, Tyler IM (1996) Tectonic evolution of Proterozoic Australia. Tectonics 15(6):1431–1446

Medaris LG, SInger BS, Dott RH, Naymark A, Johnson CM, Schott RC (2003) Late Paleoproterozoic climate, tectonics, and metamorphism in the Southern Lake Superior Region and Proto-North America; evidence from Baraboo interval quartzites. J Geol 111:243–257

Money RJC (1968) The Wollaston Lake fold–belt system, Saskatchewan–Manitoba. Can J Earth Sci 5:1489–1504

Mosher S (1996) Grenville orogenesis along the southern margin of Laurentia. Abstr Programs Geol Soc Am 28(1):55

Nyman MW, Karlstrom KE, Kirby E, Graubard CM (1994) Mesoproterozoic contractional orogeny in North America: evidence from ca. 1.4 Ga plutons. Geology 22:901–904

Onstott TC, Peacock MW (1987) Argon retentivity of hornblendes: a field experiment in a slowly cooled metamorphic terrane. Geochim Cosmochim Acta 51:2891–2903

Pagel M, Poty B, Sheppard SMF (1980) Contribution to some Saskatchewan uranium deposits mainly from fluid inclusions and isotopic data. In: Ferguson S and Goleby A (eds), Uranium in the Pine Creek Geosyncline: Vienna, International Atomic Energy Agency, p 639–654

Philippe S, Lancelot JR, Clauer N, Paquet A (1993) Formation and evolution of the Cigar Lake uranium deposit based on U–Pb and K–Ar isotope systematics. Can J Earth Sci 30:720–730

Quirt D (1997) Chloritization below the Dawn Lake uranium deposit (11A zone), northern Saskatchewan. Geological Association of Canada—Mineralogical Association of Canada Conference Abstracts 22:A-122

Ramaekers P (1990) Geology of the Athabasca Group (Helikian) in Northern Saskatchewan. Saskatchewan Energy and Mines, Saskatchewan Geological Survey, Report 195:48

Ramaekers P, Dunn CE (1977) Geology and geochemistry of the eastern margin of the Athabasca Basin. In: Dunn CE (ed) Uranium in Saskatchewan. Saskatchewan Geological Society Special Publication 3:297–322

Robertson DS, Tilsey JE, Hogg GM (1978) The time-bound character of uranium deposits. Econ Geol 73:1490–1499

Roddick JC (1983) High precision intercalibration of $^{40}Ar/^{39}Ar$ standards. Geochim Cosmochim Acta 47(5):887–898

Romano D, Holm DK, Foland KA (2000) Determining the extent and nature of Mazatzal-related overprinting of the Penokean Orogenic belt in the southern Lake Superior region, north-central USA. Precambrian Res 104:25–46

Sibbald TII (1978) Uranium metalogenic studies: Rabbit Lake geology. In: Summary of investigations 1978, Saskatchewan Geological Survey, Saskatchewan mineral resources. Miscellaneous report 78–10:56–60

Sibbald TII, Quirt D (1987) Uranium deposits of the Athabasca Basin. Geological Association of Canada, Annual Meeting, Saskatoon, 1987. Field trip guidebook. Trip 9: Saskatchewan Research Council Publication R-855-1-G-87

Sims PK, Stein HJ (2001) Tectonic history of the Proterozoic Colorado Province, Southern Rocky Mountains. Abstr Programs Geol Soc Am 33(5):4

Steiger RH, Jåger E (1977) Subcommission on geochronology: convention on the use of decay constants in geo- and cosmochronology. Earth Planet Sci Lett 36:359–362

Wallis RH (1971) The geology of the Hidden Bay area, Saskatchewan. Saskatchewan Geological Survey Report 137, 75 pp